CrossMark

Preliminary design of a small-sized flapping UAV: II. Kinematic and structural aspects

F. Negrello · P. Silvestri · A. Lucifredi ·
J. E. Guerrero · A. Bottaro

Abstract The design of the actuating mechanism of a biologically inspired flapping wing UAV is addressed. Several configurations able to reproduce the desired flapping-wing kinematics are analyzed and an optimization study is conducted to select the best configuration. The optimization results are used as the starting point for the design of the different structural components of the flapping mechanism. During the mechanism design stage, the linkages are optimized to match the desired wing's motion during a flapping cycle. A structural and durability analysis is then conducted to verify that the mechanism and its components are able to withstand the aerodynamic and inertial loads.

Keywords Flapping UAV · Biomimetics · Structural design · Flapping mechanism

F. Negrello
Department of Advanced Robotics, Istituto Italiano di Tecnologia, 30 via Morego, 16163 Genoa, Italy
e-mail: francesca.negrello@iit.it

P. Silvestri · A. Lucifredi
DIME, University of Genoa, 15 A via all'Opera Pia, 16145 Genoa, Italy

J. E. Guerrero · A. Bottaro (✉)
DICCA, University of Genoa, 1 via Montallegro, 16145 Genoa, Italy
e-mail: alessandro.bottaro@unige.it

1 Introduction

Recently, the engineering community has seen renewed interest in the low Reynolds number aerodynamics of flapping wings for lift and thrust generation, and this is chiefly due to the growing interest of developing Unmanned-Aerial-Vehicles (UAVs), Micro-Air-Vehicles (MAVs) and, more recently, Nano-Air-Vehicles (NAVs). These vehicles may use or take advantage of such unconventional propulsion and lift generation methods (such as rigid and flexible flapping wings, counterphase dual oscillating wings, ducted-tip propeller/fan, and cyclic pitch propeller) in order to achieve better performances than traditional methods.

UAVs, MAVs and NAVs are flying vehicles that are remotely controlled or can fly autonomously based on pre-programmed flight plans. These vehicles can perform surveillance and reconnaissance missions, sensing at remote or hazardous locations, traffic monitoring, forestry and wildlife surveys, inspection of power lines and aerial photography, among other tasks.

In conventional man-made flying vehicles the wings provide the lift and the engines provide the thrust. In a bird, however, the wings have to provide the thrust as well as the lift, with the added complication that they are also used to maneuver. Birds are amazing examples of unsteady aerodynamics, high maneuverability, endurance, flight stability and control, and large aerodynamic efficiency.

A UAV that resembles a bird (a biomimetic UAV), experiences the same low Reynolds number as their biological counterparts, typically in the order of 10^3–10^5; in this regime fixed wings drop dramatically in aerodynamic performance. At these low Reynolds number values, the fluid flow is prone to separation, resulting in increased drag and loss of efficiency. Even without flow separation, the low Reynolds number results in low lift-to-drag ratio due to the thickness of the boundary layer. It becomes clear that in order to develop a practical biomimetic UAV, new ways of generating lift and thrust must be investigated with the aim of overcoming the drawbacks of fixed wings at low Reynolds number.

The most common way of producing rotating, oscillating or reciprocating motion, and hence flapping motion, is the four-bar linkage mechanism. Madangopal et al. [1], Malik et al. [2] and Zbikowski et al. [3] addressed the design, implementation, and testing of four-bar linkages for flapping MAVs. Another example can be found in a patent by Kempf [4], where he describes a mechanism that generates a rigid flapping couple with a twist of the wing in a purely mechanical way and without the need of using servo-actuators. The flapping motion is generated by a slider-crank linkage, with the slider connected to the wings. To twist the wing, a second slider-crank mechanism is used with a different phase angle, equal to the desired torsion angle.

A pioneer in the studies of mechanical flapping-flight is DeLaurier [5–8], who in the 1980s and 1990s conducted a series of experiments to assess the feasibility of mechanical, powered, flapping-wing aircraft (the so called *ornithopter*). As a culmination of two decades of research, DeLaurier successfully conducted flight tests of a remotely controlled scaled proof-of-concept model which provided the key analytical tools for assessing the feasibility of the full-scale aircraft [8].

Recently, a team of researchers of the Festo company developed a prototype of a robotic seagull named Smartbird [9, 10]. The salient feature of this robotic prototype, is the use of active torsion of the wings: during the downstroke, at the bottom-most position, the angle of attack of the wings changes rapidly from negative to positive (and viceversa during the upstroke, at the top-most position) to enhance lift and thrust. Although the results presented by Send et al. [10] are impressive, some issues remain unanswered, such as the number of degrees of freedom required for the wing kinematics to yield efficient flight or the durability and structural limits of the flapping mechanism and wing structure.

When designing a biomimetic flapping UAV, we should address the aerodynamic performance of the flight vehicle, as well as the static and dynamic stability, the design of the flapping mechanism, the structural integrity of the flight vehicle components, and the mechanical performance of the flapping UAV. Hereafter, we focus our attention on the design of the flapping mechanism and its different structural components. We also conduct a structural and durability analysis to verify that the mechanism and its components are able to withstand the aerodynamic and inertial loads. The computation of the aerodynamic loads to be used in the structural study and the design of the kinematics is addressed in reference [11].

The remainder of this manuscript is organized as follows. In Sect. 2 we briefly review the design specifications, the *avian model* and design assumptions. In Sect. 3 we briefly discuss the wing kinematics and the identification of the design variables of the mechanism. In Sect. 4 we discuss the required degrees of freedom for the proposed flapping kinematics and the synthesis of the wing actuation mechanism. Section 5 describes the optimization of the mechanism linkages, while Sect. 6 shows the evaluation of the motor torque requirements. In Sect. 7 the mechanism structural design and its limits are discussed. In Sects. 8 and 9 we report the results on the durability analysis and the vibrations excited during the wing flapping, respectively. Finally, in Sect. 10 conclusions and perspectives are outlined.

2 Design specifications, avian model and design assumptions

In Table 1, the design specifications of the proposed biomimetic flapping UAV are shown. One important design specification to highlight is that the flapping frequency can be modulated, but shall not exceed 3.0 Hz; this constraint is imposed for mechanical, structural and energy-consuming reasons. It is also interesting to point out that the vehicle is intended to be hand launched with a minimum velocity of 5.0 m/s.

Table 1 Design specifications

Maximum mass	1.0 kg
Maximum flapping frequency	3.0 Hz
Minimum velocity (hand launch velocity)	5.0 m/s
Maximum velocity	14.0 m/s
Autonomy (battery life)	20.0 min

We then proceed to look for birds that closely match the specifications outlined in Table 1. The model shape, size, and flight conditions are chosen to approximate those of the gulls family. In reference [11] the full details of this study are explained. Also, the initial sizing and the layout of the *avian model* is presented. In particular, the total wing span is equal to 2.0 m.

It is important to stress that the flapping frequency is the most limiting design variable. The final configuration of the flapping mechanism and the design of the wings structural components (therefore the final weight) depend on this design parameter. High flapping frequency values imply high aerodynamic loads, high inertial loads and increased energy consumption.

Hereafter, we list a few design assumptions used during this study:

- The wings are considered to be made of two parts, one internal semi-wing and one external semi-wing. The wings are articulated at the joints between the semi-wings.
- The *avian model* and its individual components are treated as rigid bodies.
- The components of the mechanism (crank, electrical motor, gearbox, batteries, levers, etc.) are housed in the fuselage. The fuselage is assumed to have a light shell making it look like a bird.
- The wings cross section is the high-lift airfoil Selig 1223 and it is assumed that the flapping mechanism fits within the wing thickness.
- The wings motion can be represented by two degrees of freedom, namely, flapping and spanning.
- The wings have low inertia.

Of the previous design assumptions, the most prohibitive one is the restriction related to fact that the flapping mechanism must fit within the wing thickness. During the structural design phase, it might

happen that in order to withstand the aerodynamic loads, the thickness of the components of the flapping mechanism is locally larger than the maximum thickness of the wing, hence this will require a slight modification of the wing and this in turn might affect the aerodynamic performance of the *avian model*.

3 Wing kinematics

From a kinematic point of view, birds' wings have four degrees of freedom (DOF), namely:

- Flapping: which is the angular motion about the aircraft axis. This DOF generates a rolling motion of the wings.
- Lagging: which is the angular motion about a vertical axis. This DOF generates a back and forth motion of the wings.
- Feathering: which is the angular motion about an axis perpendicular to the plane generated by the axes of the flapping and lagging motions. This DOF generates a variation of the wings angle of attack.
- Spanning: which is the enlargement and contraction motion of the wings. This DOF implies that the wings are articulated and can fold.

In this study, we consider that the wings motion only exhibits two DOF, namely, flapping and spanning. According to Guerrero et al. [11], the most important variables to consider for the design of the flapping mechanism are:

- A_{iw}: which is the maximum roll amplitude of the internal semi-wing.
- A_{ie}: which is the maximum angle between the internal semi-wing and the external semi-wing.
- S: which is the fraction of time used during the upstroke. This value varies between 0 and 1. A value of 0.6, for example, means that 60 % of the flapping period is used for the upstroke; consequently, the angular velocity of the wing is lower during the upstroke.

The kinematics described in reference [11] is obtained after an extensive campaign of computational fluid dynamics (CFD) simulations. The kinematics used by Guerrero et al. [11], apart from the fact that it generates thrust and enough lift to keep the *avian model* aloft, might not be optimal from an

aerodynamic point of view. Nevertheless, this kinematics is used as the starting point for the design and sizing of the flapping mechanism and structural components.

4 Synthesis of the flapping mechanism

To synthesize the flapping mechanism, we use as design parameters the variables shown in Table 2, where A_{iw} is the maximum stroke angle or roll amplitude of the internal semi-wing and A_{ie} is the maximum angle between the internal semi-wing and the external semi-wing, as illustrated in Fig. 1. S is the fraction of time used during the upstroke.

Considering the possible combinations of stroke angles and flapping frequencies, the inertia of the wings should be low enough to ensure that the batteries can operate for a sufficiently long time; therefore, it is required to position inside the fuselage of the *avian model* the mass related to the active actuation of the flapping mechanism, i.e., the electrical motor and the gearbox. It is also required to have a light wing structure. On the other hand, the wings must be sufficiently robust to withstand the aerodynamic and inertial loads.

The goal is to design a mechanism that couples the two DOF of the wing motion (flapping and spanning) into one mechanical DOF, by using a mechanical linkage that respects the design constrains given in Table 2. Additionally, the mechanism must fit within the fuselage and wings, i.e., it must respect the geometrical constraints.

A number of mechanism derived from research project[12], patents [4, 13] and hobby hand-crafts [4, 14, 15] have been analyzed. The most used mechanism for such size of flapping wings UAVs is the fourbar linkage. The four-bar mechanism provides kinematic pairing, good behavior at high speed and does not suffer of wear problems caused by elevated contact

Table 2 Design parameters for the flapping mechanism

A_{iw}	$\approx 60°$
A_{ie}	$45° \leq A_{ie} \leq 50°$
S	$0.5 \leq T_{cycle} \leq 0.65$

forces. The considered mechanisms have a single DOF wing coupled in some cases with an elastic structure. The benefits of an articulated wing (2 DOF), from an aerodynamic point of view, justify our mechanism selection. Thus the minimum number of binary members required to design the flapping mechanism for each semi-wing is four.

The configuration chosen for the four-bar linkage that drives the internal semi-wing is the crank-rocker type, which has as input the continuous rotational motion of the electrical motor and as output an oscillating moving arm. This mechanism is designed according to the Grashov rule [16]. For the external semi-wing, a double rocker configuration is adopted (non-Grashov condition). The wing structure, is attached to one of the rockers of the external wing and to the rocker of the internal wing.

In summary, the flapping mechanism consists of two four-bar linkage in a serial configuration, where the conrod of the first four-bar linkage is the input of the second linkage.

Using Fig. 2 as a reference, the length of the first member of the first four-bar linkage is indicated with l_1 (this first member will be henceforth denoted with the subscript 1, and similarly the other parts of the mechanism). In the same way, the length of the input crank is indicated with l_2, the length of the conrod is denoted with l_3, and the length of the rocker is denoted with l_4. For the second four-bar linkage, we indicate with l_5 the length of the rod, with l_6 the length of the output rocker 6, with l_7 the length of the input rocker 7, and with l_8 the length of the rod 8.

5 Optimization of the kinematic model

The parameters of interest for describing the flapping motion are A_{iw} and A_{ie}. For the preliminary sizing of the mechanism, we express the dependency of these variables in function of the lengths l_2, l_3, and l_4, as follows:

$$A_{iw} = f(l_2, l_4); \tag{1}$$

$$A_{ie} = f(l_2, l_3). \tag{2}$$

The length l_1 does not appear as it is used as a normalization parameter for the mechanism. By using equations 1 and 2, we can proceed to find the initial
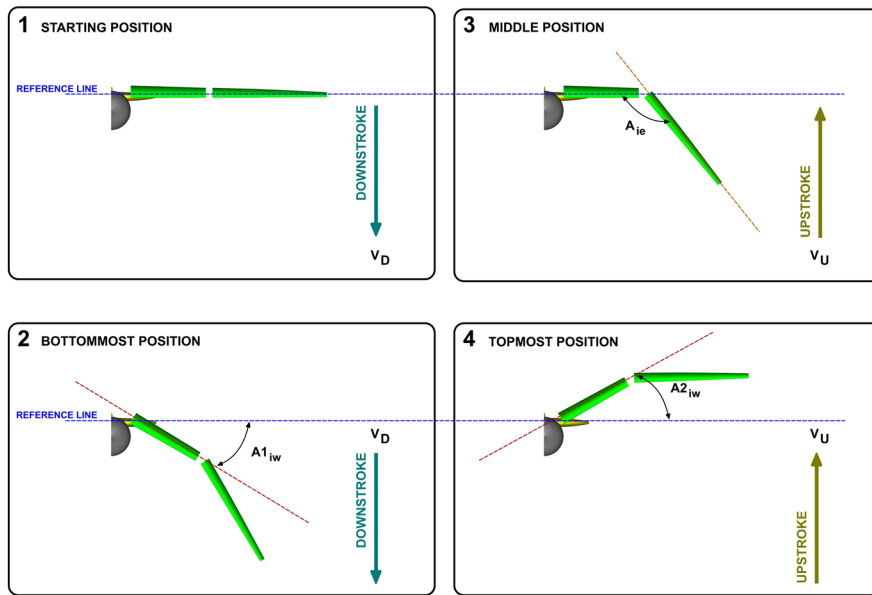
Fig. 1 Illustration of the wing kinematics and design variables. $45° \leq A_{ie} \leq 50°$, $A1_{iw} = A2_{iw} = A_{iw}/2 \approx 30°$, $V_U = V_D$. The sequence is from **1** to **4**, where **1** is the starting position, **2** is the bottom-most position, **3** is the mid-position during the upstroke, and **4** is the top-most position

Fig. 2 Schematic representation of the flapping mechanism
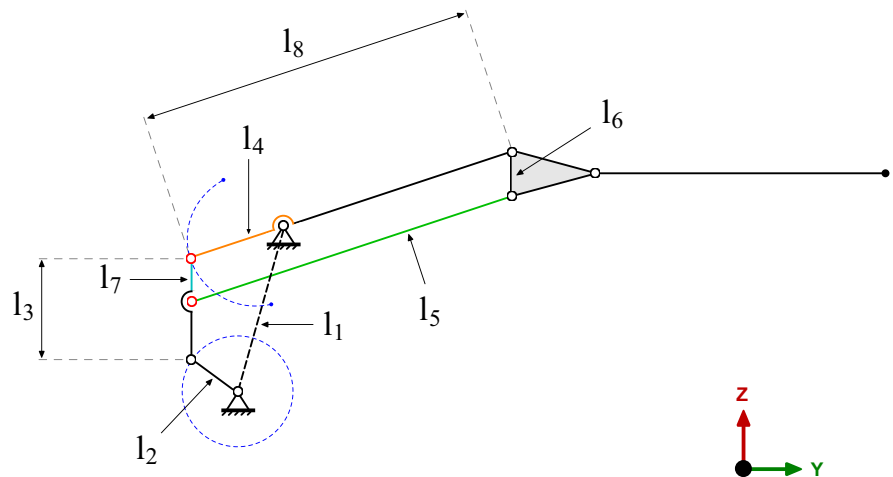
lengths of the links 1, 2, 3, and 4 (refer to Fig. 2); these initial values must respect the kinematics and geometrical constrains. Then, these initial values are used as starting point for the optimization study, where we aim at obtaining the optimal length of the members of the mechanism that reproduce with the minimum error the wing kinematics described in reference [11].

For the optimization study, we use the optimization package integrated in the multi-body dynamics software LMS Virtual.Lab [17, 18]. Inside LMS Virtual.Lab, we proceed to create a parametric model representing the length of the members with the mechanical and geometrical constraints. The problem is fully decoupled since the variables of each semi-wing are independent, so it is possible to perform the optimization of each mechanism in two separated steps. The driver of the motion is the crank, and the angles of the internal semi-wing and external semi-

wing are those between the links 1–4 (A_{iw}) and 4–6 (A_{ie}), respectively.

For the optimization study of the internal wing, the design variables are A_{iw} and S (refer to Table 1). In this optimization problem we evaluate A_{iw} as follows:

$$A_{iw} = A_{iw}^T - A_{iw}^B = \left\{ \arccos \left[\frac{(l_4^2 - (l_3 + l_2)^2 + l_1^2)}{(2l_1l_4)} \right] - \arccos \left[\frac{(l_4^2 - (l_3 - l_2)^2 + l_1^2)}{(2l_1l_4)} \right] \right\} \frac{360°}{2\pi};$$ (3)

this equation is derived by taking the difference of the angular position of the rocker belonging to the internal wing at the top-most (A_{iw}^T) and bottom-most positions (A_{iw}^B).

The first objective function for the optimization of the mechanism of the internal semi-wing is the error ε_1 defined as,

$$\varepsilon_1 = (A_{iw} - 60°)^2.$$ (4)

The flapping period and the crank positions θ_2^T and θ_2^B are correlated; in our discussion θ_2^T corresponds to the top-most position of the rocker and θ_2^B corresponds to the bottom-most position. Then, the angular range θ_2 defining the input crank rotation during the upstroke is defined as,

$$\theta_2 = \theta_2^T - \theta_2^B = \left\{ \arccos \left[\frac{(-l_4^2 + (l_3 + l_2)^2 + l_1^2)}{(2l_1l_4)} \right] - \arccos \left[\frac{(-l_4^2 + (l_3 - l_2)^2 + l_1^2)}{(2l_1l_4)} \right] \right\} \frac{360°}{2\pi} + 180°;$$ (5)

this equation is derived by taking the difference of the angular position of the input crank at the top-most position (θ_{iw}^T) and bottom-most position (θ_{iw}^B) of the internal wing.

To obtain different angular velocities during the upstroke and down-stroke, we use the design variable S which is in the range $50\% \leq S \leq 65\%$.

Then, the second objective function is defined as

$$\varepsilon_2 = (\theta_2 - S \times 360°)^2,$$ (6)

where we use four values for S, namely: 50, 55, 60 and 65%. At this point, we can start the multi-objective optimization study, where the goal is to minimize the value of ε_1 and ε_2.

For the two objective functions related to the internal semi-wing, a DOE (design of experiment) is performed, where the lower limits of the design variables are defined in terms of the structural strength. The choice of the upper limits is dictated by the maximum physical dimensions allowed (geometrical constraints). Then the optimization is performed by using a gradient based Pareto-set method, where we give different weights to the individual objective functions and the collection of computed optimal solutions form a Pareto set. The two objective functions are competitive, i.e., optimizing the first objective function generates a larger error in the second objective function. As a consequence, the best results are obtained when a large weight is given to the second objective function. The final results of this study are presented in Tables 3 and 4, where in Table 3 we show the error between the final result and the target value; and in Table 4 we show the optimal values for the lengths l_2, l_3, and l_4.

For the external semi-wing, the optimization problem is related to the relative angle between the two semi-wings A_{ie}; hence, this is a single-objective optimization problem. The first member of the second four-bar linkage is part of the conrod 3 of the first four-bar linkage. The optimization variables are the rod length l_5, the rocker length l_6, and the position of the

Table 3 Comparison between the design goals and the results obtained via optimization for $S = 60\%$

Objective function	Target value	Final value	Error %
A_{iw}	60°	60.022°	≈ 0.035
θ_2	234°	234.017°	≈ 0.007

Table 4 Optimal length and angular values of the different links of the mechanism

Design variable	Initial value (mm)	Optimal value (mm)
l_1	50.367	50.36
l_2	$24 \leq l_2 \leq 26$	25.10
l_3	$48 \leq l_3 \leq 50$	48.08
l_4	$62 \leq l_4 \leq 64$	62.48
l_5	–	457.0
l_6	–	25.0
θ_2 (°)	–	15° + 180°

pivots of the second four-bar linkage on link 3 (shown in red in Fig. 2).

The objective function for this optimization problem does not consist of an error but directly in the expected value of the design variable A_{ie}, which should be in the range $45° \leq A_{ie} \leq 50°$. Considering the dimensions of the flight vehicle [11], and since the mechanism must fit inside the wing structure, the best four-bar linkage would be the parallelogram with parallel bars during the entire stroke; however, with this choice the relative angle is fixed and if we scale the length of the parallelogram, A_{ie} does not vary. Instead, considering a four-bar linkage where l_8 and l_5 are slightly different, has a direct effect on the objective function A_{ie}. Therefore, this solution is adopted taking as design variables l_6, l_5, and the angle between the conrod l_3 and the rocker l_7 (the angle θ). The remaining lengths are chosen in such a way as to reduce as much as possible the physical dimensions of the mechanism, hence keeping weight to a minimum.

The objective function related to A_{ie} is again computed using the multi-body dynamics software LMS Virtual.Lab [18], where a virtual model of the system kinematics is created. To compute the relative angular velocity we define a virtual angular velocity sensor on the members under consideration (l_6 and l_8), and then we integrate the output of the virtual sensor over a period of oscillation. The range of acceptability of the maximum relative angle between the two semi-wings is the result of a compromise between the aerodynamic requirements and the structural strength of the real components.

This objective function (which expresses the relative angle between the two semi-wings), when applied to the four-bar mechanism, is proportional to l_6 and inversely proportional to the angle θ. The parameter l_5 is chosen so that the relative angle falls within the desired range.

To solve this optimization problem, we use again a gradient based method. The solution does not present convergence issues, since the starting configuration is not far from the optimal value. Table 5 summarizes the optimal solution achieved.

6 Motor selection and torque profile

To determine the torque that the motor has to supply to the mechanism several simulations on the selected

Table 5 Comparison between the design goals and the results obtained via optimization

Objective function	Target value	Best value
A_{ie}	$45° \leq A_{ie} \leq 50°$	$47.7°$
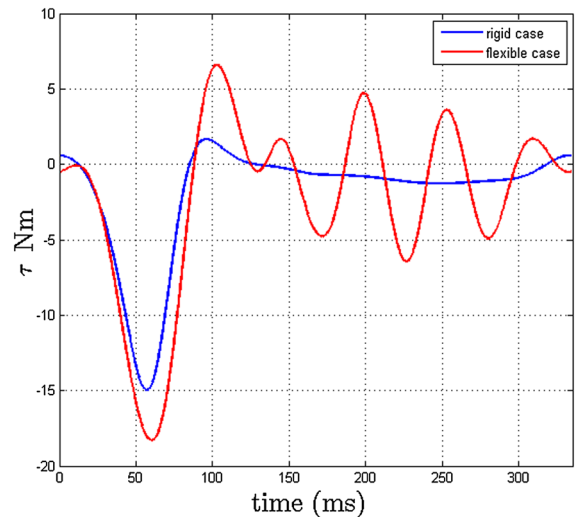
Fig. 3 Torque of the mechanism for one flapping cycle imposing $\omega = 180$ rpm, in *blue* the rigid case, in *red* the flexible case. (Color figure online)

configuration have been conducted. Firstly, peak and averaged torque, on the motor side, have been estimated imposing an ideal velocity driver ($\omega = 180$ rpm). For the sizing of the motor we considered the worst case scenario, which implies that we applied to the wing the aerodynamic load at the maximum speed and at the maximum flapping frequency (14 m/s; 3 Hz).

In Fig. 3 the torque trend over time for one flapping cycle is displayed, for both the rigid (blue) and the deformable case (red curve with oscillations); for this latter configuration refer to further Sect. 7 where the finite element analysis of the mechanism is described. Peak torque is about 20 Nm, averaged torque is 2.23 Nm, while the RMS torque is 6.22 Nm. Comparing the torque curves in Fig. 3, the elasticity of the wing introduces more oscillation in the torque profile with respect to the rigid case. While these small oscillations are not significant for the estimation of the averaged torque level, they should be considered when evaluating the peak torque and the performances of the selected drive-train (motor and gearbox).

To estimate the reduced inertia to be added to the model, it is necessary to identify a drive-train that matches the system requirements: $\tau_{peak} = 0.2$ Nm for a reduction ratio between 80 and 100 (harmonic drive), $\omega = 180$ rpm. An electrical motor has been selected from a commercial catalogue [19] with the following characteristics: $\tau_{peak} = 0.106$ Nm, $\omega = 13,100$ rpm. Thus, the reflected inertia is evaluated to be about 35×10^{-3} kgm^2.

To evaluate the effective performances of the mechanism, simulations have been conducted having as input the torque characteristic of the selected motor and gearbox. In Fig. 4 the torque trend over time for one flapping cycle is reported, for both the rigid (blue) and the deformable case (red curve with oscillations). Also in this case, it is possible to identify vibrations of the linkages excited by the flapping frequency and the applied loads in the deformable configuration. Thus, the (conservative) flexible case should be considered as reference for the motor sizing. Moreover, it is worth noticing that applying a real input to the system, the elasticity of the linkages introduces a delay in the system response (Figs. 4, 5). In Fig. 5 the angular velocity trend over time for one flapping cycle is reported, for both the rigid (blue) and the deformable (red) case. In conclusion, simulations show that even though the motor torque saturates, the designed system

is apt to reproduce the desired flapping motion with an average angular velocity of $\omega = 176$ rpm that is to within 2 % of the requirements.

7 Design goal and structural analysis

The system under consideration is a compromise between weight, aerodynamic performance and structural strength, as the final goal is to design a biomimetic flapping UAV able to generate lift and thrust and, at the same time, the flapping mechanism and wing structure must withstand the aerodynamic and inertial loads of the flapping motion.

To conduct the preliminary structural study, we use aluminum as a standard material for the mechanism. In Table 6, the aluminum material properties used in this
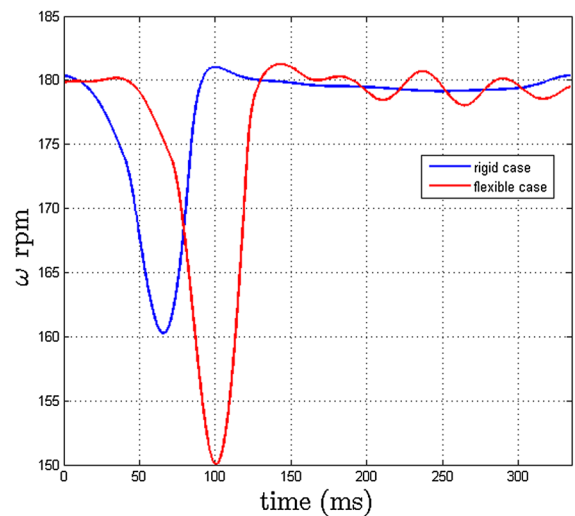
Fig. 5 Angular velocity of the mechanism for one flapping cycle imposing a real motor torque characteristic, in *blue* the rigid case, in *red* the flexible case for which the minimum rpm is found at 100 ms. (Color figure online)

Table 6 Aluminum material properties

Material property	Value
Young modulus (E)	7×10^4 MPa
Poisson ratio (v)	0.346
Density (ρ)	2710 kg/m^3
Yield strain ($R_{p0.2}$)	440 MPa
Ultimate strain (R_m)	500 MPa

Fig. 4 Mechanism torque for one flapping cycle imposing a real motor torque characteristic, in *blue* the real case, in *red* the flexible case. (Color figure online)
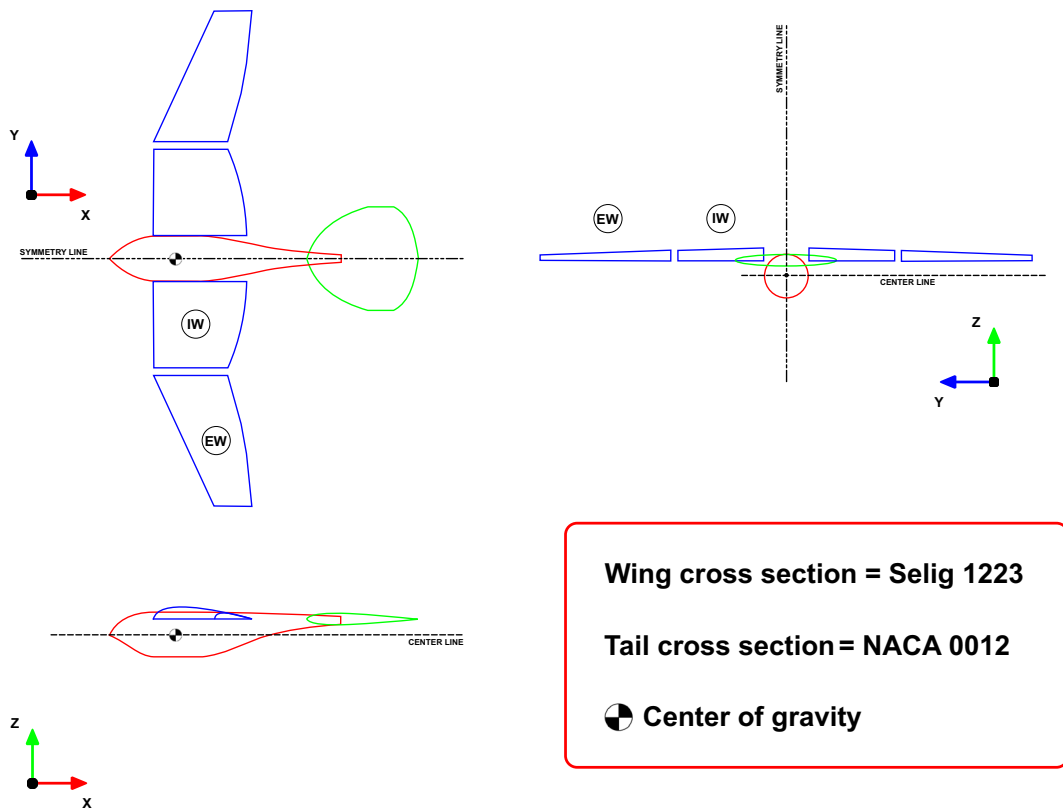
Fig. 6 Three-view of the avian model. In the figure, EW stands for external semi-wing, and IW stands for internal semi-wing

study are reported. The material is assumed to be homogeneous and isotropic.

From the point of view of the structural design of the mechanism, we want a light and strong structure. To achieve the structural strength requirements a static structural analysis is carried out, where we initially assume that the loads are constant and equal to the maximum value of the aerodynamic loads plus the inertial loads contribution, during a flapping cycle at maximum frequency and maximum velocity (worst case scenario). After verifying that the structure resists the maximum static loads, an optimization study of the single components of the mechanism is carried out using the dynamic loads during a flapping cycle. The aerodynamic loads are those obtained from the aerodynamic study [11] and the inertial loads are obtained using a multi-body dynamics approach. With reference to the axes shown in Fig. 6, the loads which mainly affect the mechanism are:

- Primary bending of the wing in the $y - z$ plane, as a consequence of the inertial and aerodynamic loads

due to the flapping motion. To minimize the strain and deflections due to the loads, it is appropriate to use sections with high moment of area.
- Secondary bending of the wing in the $x - y$ plane, as a consequence of the aerodynamic loads. To minimize this effect without penalizing the weight constraint, a ribbed structure with two light spars is used, creating in this a way a wing-box.
- Torsion around y axis, caused by asymmetric pressure distribution on the wing surface and possible misalignment between the center of mass and the center of pressure of the wing, when the wing is articulating. To minimize the torsion, we can move the front spar closer to the center of pressure. However, this is difficult to obtain due to geometric constraints.

To better understand what components of the mechanism are more critical (in terms of structural loads), hereafter we give a brief description of the mechanical parts and the principal design choices.

The electrical motor is connected to the crank (2 in Fig. 2) by a gearbox; in this design the crank is modeled as a gear with lightening holes to make the structure lighter. To achieve a 3.0 Hz flapping frequency, the angular velocity of the crank is set to 180 rpm. During the simulations, this value is reached after a short transient. The crank is comparable to a beam with two revolute joints at the ends, and the loads are mainly distributed along the axis; there is also a secondary component of bending because the joints are not aligned on the same plane.

The conrod (3 in Fig. 2) is the link between the motor input and the internal semi-wing. It is responsible for extending and retracting the wing during the down-stroke and upstroke. This part is made as light as possible by using lightening holes. Tri-axial loads act on the conrod.

The internal semi-wing is attached to the rocker (4 in Fig. 2); it is designed to resist the aerodynamic and the inertial loads (dynamic and static) exerted on it.

The spar (5 in Fig. 2) transmits the motion to the external semi-wing, generating the retraction and extension of the wing during the upstroke and down-stroke, respectively. It helps the mechanism resist primary bending; for this reason its shape is studied to avoid buckling when the conrod is under compression (when the external semi-wing starts to extend).

The second conrod (6 in Fig. 2) represents the external semi-wing. This element is critical due to its position. It must be as light as possible for inertia consideration, but it also needs to resist bending due to the high aerodynamic loads generated by the high angular velocities.

The solver used for this study, is based on the Craig-Bampton algorithm for the superposition of modal forms [20]. To account for the modal superposition it is necessary to evaluate modal participation factors of various forms. In this method, the participation factor quantify the contribution of each mode of vibration in the generation of displacements and therefore of tensions. In particular, the solver employed (LMS Samcef [22]) makes use of the following formula that expresses the combination between loads and mode shapes for the calculation of the local tensions in time:

$$\sigma_{i,j}(x,t) = \sum_k c_{ij}^{(k)}(x) L_k(t), \tag{7}$$

where $c_{ij}^{(k)}(x)$ represents the k-th mode in x and $L_k(t)$ is the k-th load at time t. The results in terms of strain are calculated according to the equivalent Von Mises stresses, at the instant when loads are maximum during a flapping cycle at maximum frequency and maximum velocity (worst case scenario).

In Table 7, the results of the structural analysis are reported. In this table, the maximum stress of each component is lower than the yield stress of the selected material, hence the structural design is suitable to work under the given operating conditions. The safety factor is defined as the ratio between the maximum stress on the component and the yield stress of the material. In the same table, the maximum displacement of the components is also reported.

Taking into account the harsh conditions under which the mechanism is working, the high aerodynamic and inertial dynamic loads due to the high flapping frequency (3.0 Hz), the stresses of the components and vibrations, it is of interest to perform more advanced studies such as, (1) a fatigue study and (2) an analysis to find the various vibration modes and the natural frequencies of the structure. These issues are addressed in the next sections.

For completeness, in Figs. 7, 8, 9, 10, and 11 we show the maximum stresses on different components of the mechanism. In Fig. 12 a 3D drawing of the proposed mechanism is displayed.

8 Durability analysis

To conduct the durability analysis to detect the degradation of the material due to repeated cyclic

Table 7 Results of the structural analysis for each element of the mechanism

Component	Max stress (MPa)	Max displacement (mm)	Safety factor
Crank (l_2)	300	–	1.47
Conrod (l_3)	260	–	1.69
Rocker (l_4)	200	4.75	2.2
Spar (l_5)	280	2.55	1.57
Second conrod (l_6)	290	6.83	1.52

Fig. 7 Maximum stresses (Pa) on the external conrod during a flapping cycle
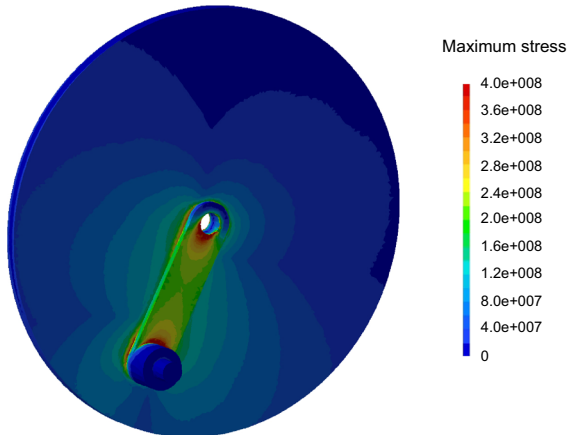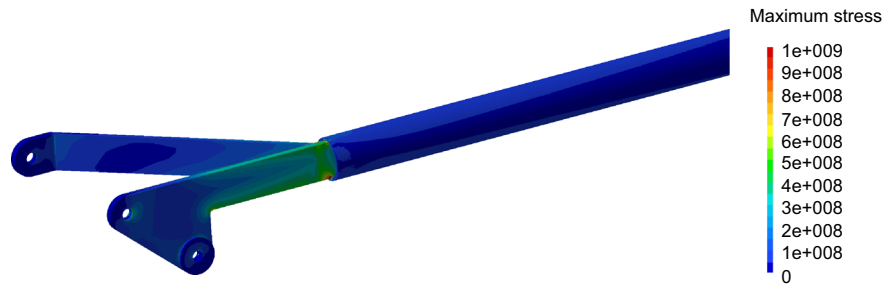
Fig. 8 Maximum stresses (Pa) on the crank during a flapping cycle

loading, the software LMS Virtual.Lab [18] is used. This software allows estimating crack initiation time by conducting an analysis of the stresses and strains in the structure. Two basic approaches are available in LMS Virtual.Lab, the stress-life approach and the strain-life approach. The stress-life approach, adopted in the present analysis, assumes that all stresses in the component are below the elastic limit of the material at all times; the approach is suitable when applied stresses are nominally within the elastic range and the number of cycles to failure is large. For further details on the technique, based on Woehler life curve an Miner's elementary accumulation rule, we refer to Stephens et al. [21].

LMS Virtual.Lab requires fatigue data in the form of stress curves against the number of stress cycles before failure occurs. This information is obtained from the database available in LMS Virtual.Lab [18], based on pre-defined tests conducted on standardized smooth specimens.

During the durability study, we consider the mechanism to be continuously operating at a flapping frequency of 3.0 Hz and maximum cruise velocity (worst case scenario). The aerodynamic and inertial loads (which are maximum), are considered to be applied at the center of pressure of the internal and external semi-wings. The maximum stress values obtained provide an indication on the most critical zones which may be subject to fatigue.

Fig. 9 Maximum stresses (Pa) on the internal wing spar during a flapping cycle
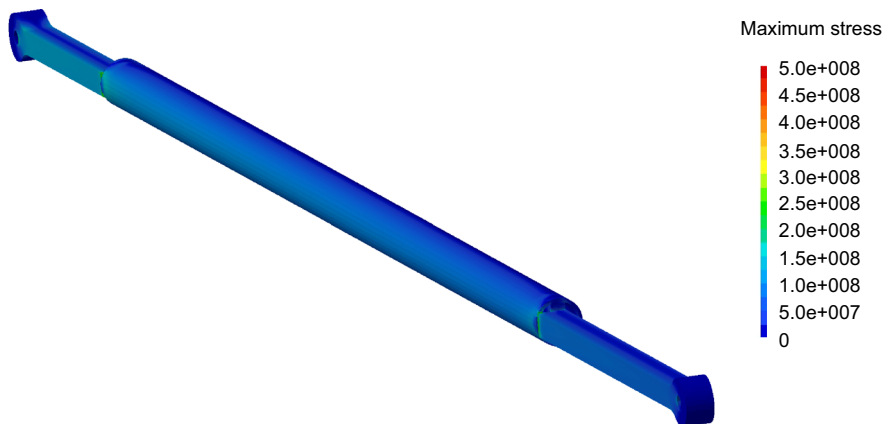
Fig. 10 Maximum stresses (Pa) on the internal conrod during a flapping cycle

Maximum stress

	2.0e+008
	1.8e+008
	1.6e+008
	1.4e+008
	1.2e+008
	1.0e+008
	8.0e+007
	6.0e+007
	4.0e+007
	2.0e+007
	0
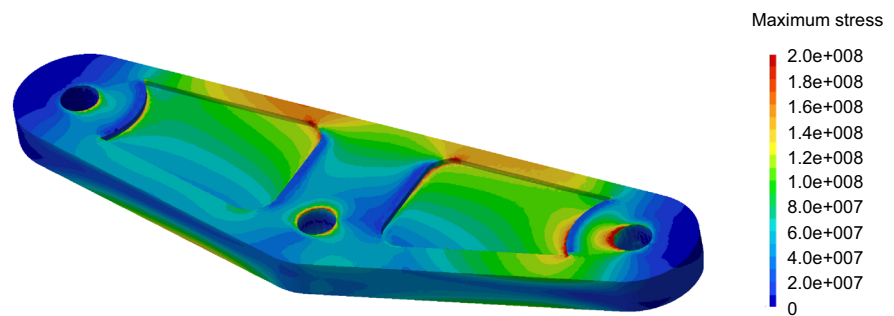
Fig. 11 Maximum stresses (Pa) on the internal wing structure during a flapping cycle

Maximum stress

	2.0e+008
	1.8e+008
	1.6e+008
	1.4e+008
	1.2e+008
	1.0e+008
	8.0e+007
	6.0e+007
	4.0e+007
	2.0e+007
	0
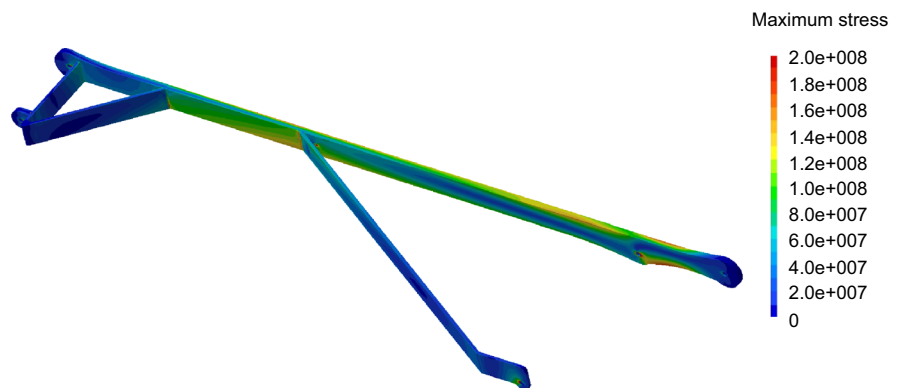
Fig. 12 Three-dimensional view of the proposed mechanism
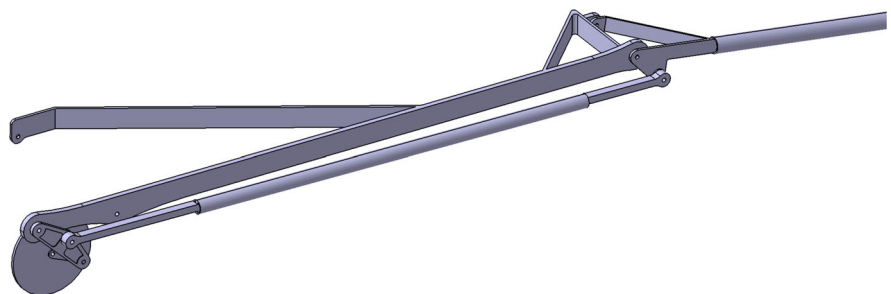
In Fig. 13, we show the results of the durability study of the input rocker, which is one of the most critical components from a structural point of view. In the figure, the scalar value *fatigue life* is an index used by LMS Virtual.Lab to represent the life of the component under the operation conditions considered, before the onset of a fatigue crack. This index is expressed as a multiple of the simulated cycle or wing flapping cycle.

By analyzing the fatigue behavior of the rocker, we can evidence the existence of critical zones, corresponding to the most stressed ones. The simulation results give fatigue life values higher than 1×10^4

cycles, this estimated fatigue life can be considered sufficient for a proof-of-concept prototype, but should be increased to match the standard fatigue life of commercial products.

Let us now analyze the crank. By looking at Fig. 14, criticalities are apparent for the fatigue life in the zone between the crank pin and the frame pin. Comparing this behavior with the one of the maximum stress (Fig. 8), it can be observe that a correlation exist between fatigue life and maximum stress values (localized in the crank pin and in the frame pin).

The external conrod (Fig. 15), is *fatigue-critical* in the sections near the hinges. As in the case of the

Fig. 13 Fatigue life of the input rocker (number of cycles). The life limited zones are colored in *red*. (Color figure online)

Fatigue life

1e+007
9e+006
8e+006
7e+006
6e+006
5e+006
4e+006
3e+006
2e+006
1e+006
1e+004

Fatigue life

1e+007
9e+006
8e+006
7e+006
6e+006
5e+006
4e+006
3e+006
2e+006
1e+006
1e+004
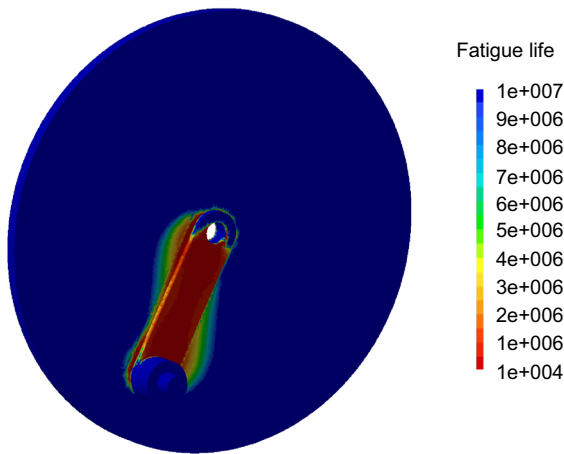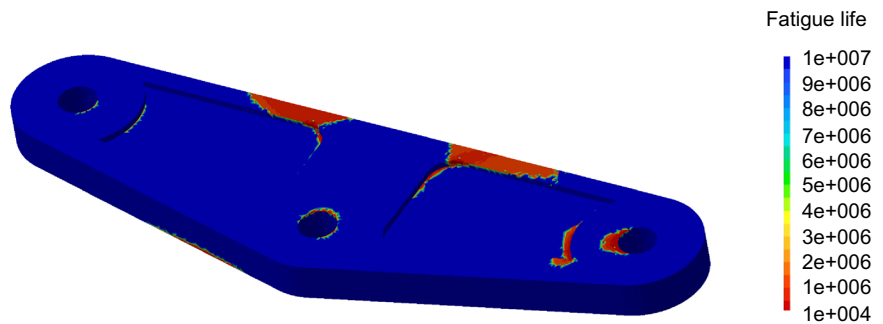
Fig. 14 Fatigue life of the crank (number of cycles). The life limited zones are colored in *red*. (Color figure online)

previous part, we are in the presence of points exhibiting high stress values and fatigue damage in the zone at the beginning of the cylindrical stiffening element.

The internal wing structure exhibits well defined zones where the fatigue damage is evident (Fig. 16). Comparing the fatigue behavior of this component with respect to the other parts of the mechanism, this component shows higher values of fatigue durability, because it withstand lower stresses (Fig. 11).

Summarizing, the frame pivot and the crank pin are the most critical in terms of fatigue; the limited values of the fatigue life time reached in these zones (lower than 2000 cycles or 600 s operating at the maximum flapping frequency of 3.0 Hz) might require a redesign of these components to render the mechanism duration acceptable. Areas of the rocker and other areas near the hinge points of the external conrod also show criticalities. It is worth stressing the fact that the

simulations are performed in the worst case scenario (highest flapping frequency and cruise velocity). Operating at lower flapping frequencies and cruise velocities will yield significant reduction of the aerodynamic and inertial loads and therefore a better fatigue behavior of the whole system.

9 Vibration modes in the different configurations of the linkage during the wing flapping

The results of a sequence of modal analyses of the mechanism in the various configurations adopted during the wings flapping cycle are reported hereafter. To get detailed information on the modal behavior during a flapping cycle, 20 different positions of the crank are considered, spaced at 18 degrees.

To conduct this study we use the simulation environment LMS Samcef [22]. In this study we link two numerical studies, namely, an implicit non-linear study and a linear modal study. The non-linear study evaluates the kinematic of the linkage for large crank rotations and the linear modal analysis is performed at the end of each instant of the non-linear study. This work flow is done in a fully automatic way.

To perform the modal analysis it is necessary to modify some constraints of the system, in particular the hinge constraint used in the linkage is substituted by a bushing joint. This is done because the hinge elements introduce a non-linear behavior incompatible with the linearization assumption adopted for the computation of the vibration modes.

The methodology adopted makes it possible to numerically evaluate how the frequency of the vibration modes varies in the different configurations adopted by the mechanism during a flapping cycle. In Fig. 17, we show the mode shapes of the first six

Fig. 15 Fatigue life of the external conrod (number of cycles). The life limited zones are colored in *red*. (Color figure online)

Fatigue life

1e+007
9e+006
8e+006
7e+006
6e+006
5e+006
4e+006
3e+006
2e+006
1e+006
1e+004
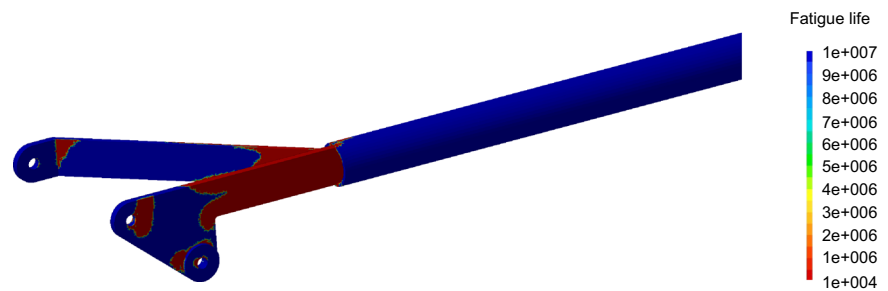
Fig. 16 Fatigue life of the internal wing structure (number of cycles). The life limited zones are colored in *red*. (Color figure online)

Fatigue life

1e+007
9e+006
8e+006
7e+006
6e+006
5e+006
4e+006
3e+006
2e+006
1e+006
1e+004
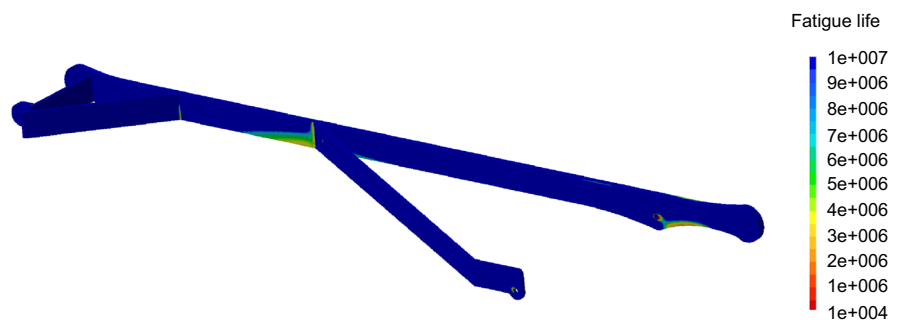
modes for a crank angle of 0 degrees. In this figure, it can be evidenced that the first two mode shapes have bending characteristics.

Let us study the mode's frequency while we vary the crank rotation angle, these results are shown in Fig. 18. In reference to the first mode (Fig. 18a), we observe that for crank angles of $0° \leq \theta \leq 150°$, the vibration frequency values are low. This may be explained due to the elevated value of the moment of inertia of the system with respect to the direction normal to the mechanism plane. The increase of the inertia implies a reduction of the vibration frequency. The same observations can be extended to the second mode (Fig. 18a), which also shows a bending mode shape.

Modes 3 and 4 (Fig. 18b), present opposite behaviors with respect to the previous modes. This may be explained by the torsional characteristics of the mode shape, the extension of the wing causes a reduction of the moment of inertia with respect to the longitudinal direction of the linkage, which explains the increase of the frequencies of the modes.

Finally, modes 5 and 6 (Fig. 18c) have mode shapes which display local bending characteristics in the internal part of the wing, in this case the low sensitivity to the inertia related to the position of the linkage in the vibration mode implies a low sensitivity of the

frequency to the variations of configuration of the linkage during the wing flapping.

Considering the frequencies of the first mode of vibration and the frequency corresponding to the wing flapping (3.0 Hz), it is possible to evaluate if resonance conditions take place in the system. Analyzing Fig. 18, which reports the fundamental frequencies in the different configurations of the linkage, we can observe that the vibration modes frequency is always higher than the flapping frequency by at least 4 times of the wing flapping frequency. Hence, it seems safe to claim that the system dynamics is acceptable, since all the modes are weakly excited.

10 Conclusions and perspectives

The work presented in this manuscript is part of an ongoing multi-disciplinary effort aimed at designing a biomimetic flapping UAV. The multi-disciplinary study includes the aerodynamic performance study, the static and dynamic stability study, the design of the flapping mechanism, the structural analysis study, and the mechanical performance study of the *avian model*.

The wing kinematics obtained from the CFD simulations is used as the starting point for the design of the flapping mechanism. An optimization study is

Fig. 17 Mode shapes of the first six modes of the mechanism for a crank position corresponding to $\theta = 0$. The first and second mode (**a** and in **b** in the figure) show bending characteristics. The third and fourth mode (**c** and **d** in the figure) shows torsional characteristics. The fifth and sixth modes (**e** and **f** in the figure) show local bending characteristics in the internal part of the wing. In the figure, the *green* shape is the undeformed geometry. The *colored shape* represents the deformed geometry (where the deformation has been amplify). (Color figure online)
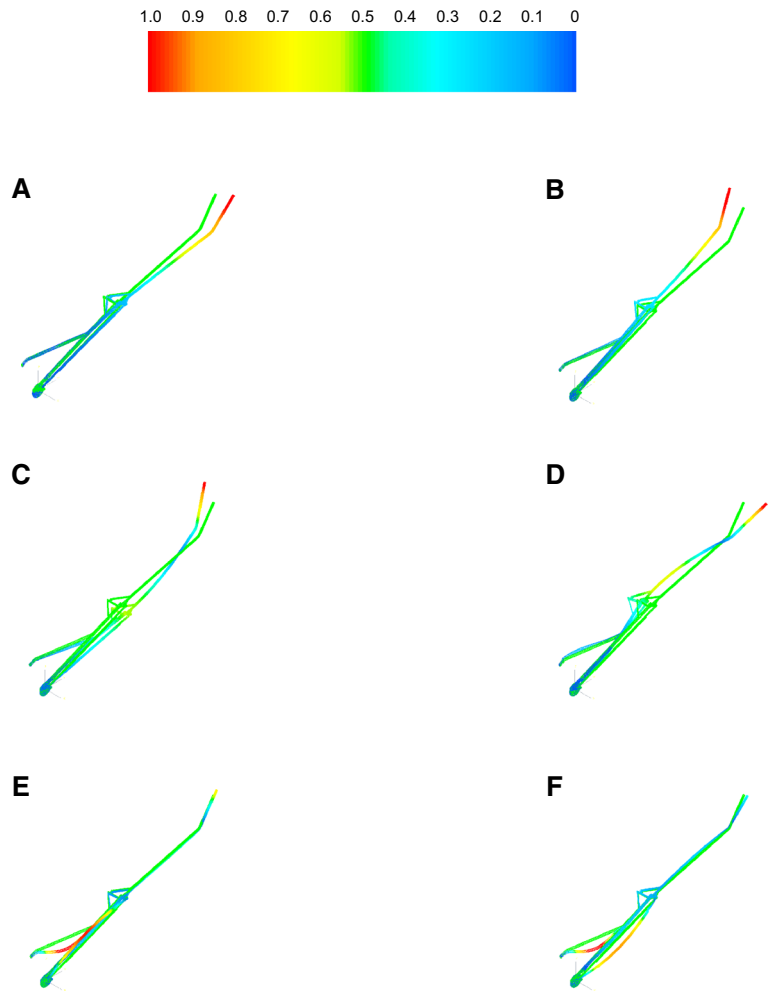
then conducted to optimize the mechanism linkages. At the end of this study, a mechanism able to reproduce the proposed kinematics has been synthesized.

The proposed kinematics resembles that of nature's fliers, produces thrust and lift, does not generate high angular velocities that could compromise the structural integrity of the *avian model* and, most importantly, we are able to design it by using a four-bar linkage.

From this study, it is found that the preliminary mechanism and structural components withstand the static and dynamic loads generated by the flapping motion. To reduce the inertia, the actuation group is located inside the fuselage which provides the flight vehicle with an aerodynamic and protective shell. The wings are designed as light and strong as possible, so they have low inertia and do not fail under the operating conditions.

The results obtained from the durability study yield fatigue life values higher than 1×10^4 cycles, the estimated fatigue life can be considered sufficient for a proof-of-concept prototype, but should be increased to get a higher fatigue life for a reusable flapping UAV or comparable commercial product. From the vibration modes study, it is found that the inertia of the wings highly influences the vibration frequencies. It is also found that we should be far from resonance conditions as the frequencies of all modes are higher that the flapping frequency.

It is envisaged to conduct a structural study using lightweight, high-strength composite materials to achieve high performances. The idea is to use carbon fiber that offers high strength-to-weight ratios. The
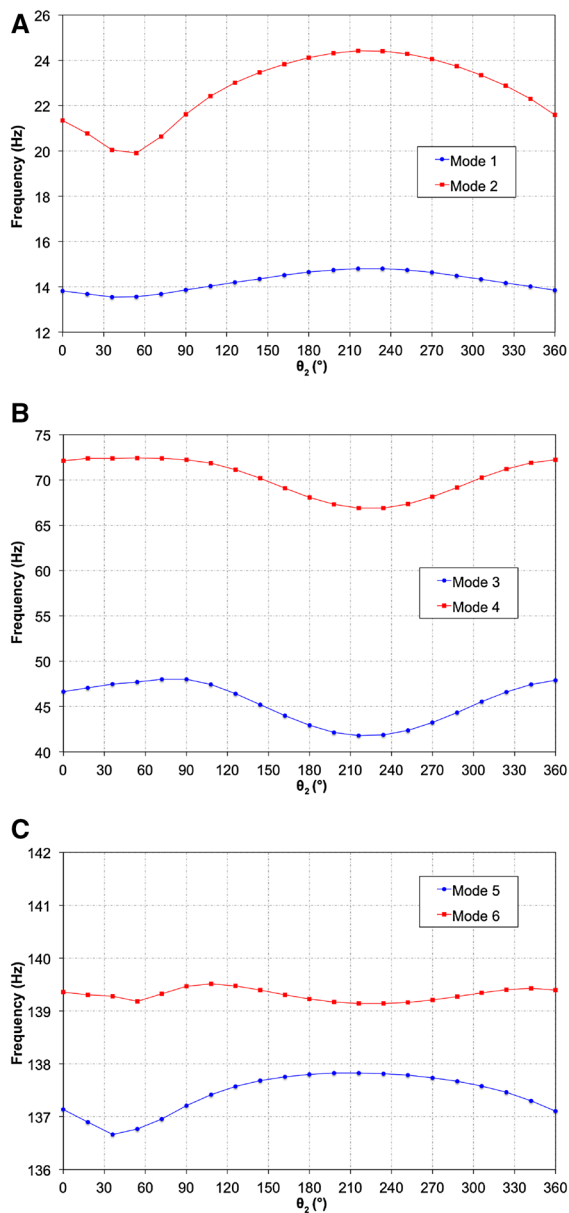
Fig. 18 Frequency variation of the vibration modes during the motion of the mechanism

CFD results, and get better estimates of the stability derivatives and aerodynamic damping coefficient in order to improve/validate the dynamic stability study and devise efficient flight control laws.

Based on the results presented, the authors believe that it is feasible to build an operational proof-of-concept model of the biomimetic flapping UAV. This represents the next step of our work.

same multi-body dynamics package used for the design of the mechanism has been employed for the dynamic stability study. While we do not present here any results of this study, for the aerodynamic damping coefficient value used it is found that the flight vehicle has an acceptable response to external perturbation and dynamic loads (aerodynamic and inertial). It is of interest to conduct wind tunnel tests to validate the

References

1. Madangopal R, Khan ZA, Agrawal SK (2005) Biologically inspired design of small flapping wing air vehicles using four-bar mechanisms and quasi-steady aerodynamics. J Mech Des 127:809–816
2. Malik AM, Khalid MSU, Barlas F (2010) Modeling and simulation of kinematics for an active flapping and pitching mechanism. In: Proceedings of the World Congress on Engineering 2010 vol II WCE 2010, June 30–July 2, 2010, London, UK
3. Zbikowski R, Galinski C, Pedersen CB (2005) Four-bar linkage mechanism for insectlike flapping wings in hover: concept and an outline of its realization. J Mech Des 127(4):817–824
4. Kempf A (1999) Patent nFR2776937, France
5. Larijani RF, DeLaurier JD (2001) nonlinear aeroelastic model for the study of flapping wing flight, fixed and flapping wing aerodynamics for micro air vehicle applications. In: Mueller TJ (ed) Progress in astronautics and aeronautics, vol 195. AIAA, Reston, pp 399–420
6. DeLaurier JD, Harris JM (1993) A study of mechanical flapping-wing flight. Aeronaut J R Aeronaut Soc 97(968): 277–286
7. DeLaurier JD (1993) An aerodynamic model for flapping-wing flight. Aeronaut J R Aeronaut Soc 97(964):125–130
8. DeLaurier JD (1999) The development and testing of a full-scale piloted ornithopter. Can Aeronaut Space J 45(2): 72–82
9. http://www.festo.com/cms/en_corp/11369.htm
10. Send W, Fischer M, Jebens K, Mugrauer R, Nagarathinam A, Scharstein F (2012) Artificial hinged-wing bird with active torsion and partially linear kinematics. Congress ICAS 2012
11. Guerrero JE, Pacioselli C, Pralits JO, Negrello F, Silvestri P, Lucifredi A, Bottaro A (2014) Preliminary design of a small-size flapping UAV. I. Aerodynamic performance and static longitudinal stability, to be submitted (2014)
12. DeLaurier J et al Ornithopter project. Available at: http://www.ornithopter.net
13. Ornithopters Patent Collection. Available at: http://www.rexresearch.com/ornithopter/ornithopter.htm
14. Kempf A, Truefly. Available at:http://truefly.chez.com
15. Kakuta K, Buteo F4. Available at: http://homepage2.nifty.com/smark/ButeoF4E.htm
16. Sclater N, Chironis NP (2001) Mechanisms and mechanical devices sourcebook. McGraw-Hill, New York

17. Schiehlen W et al (1990) Multibody systems handbook. Springer, Berlin
18. LMS Virtual Lab R12 On-Line Help, Leuven, Belgium (2013)
19. http://www.maxonmotor.it/maxon/view/catalog
20. Craig R, Bampton M (1968) Coupling of substructures for dynamics analysis. AIAA J 6(7):1313–1319
21. Stephens RI, Fatemi A, Stephens RR, Fuchs HO (2001) Metal fatigue in engineering, 2nd edn. Wiley, New Jersey
22. LMS Samcef Field 8.4 On-Line Help, Leuven, Belgium (2013)